Toxicology and Applied Pharmacology 261 (2012) 204–216

Contents lists available at SciVerse ScienceDirect

Toxicology and Applied Pharmacology

journal homepage: www.elsevier.com/locate/ytaap

Chronic occupational exposure to arsenic induces carcinogenic gene signaling networks and neoplastic transformation in human lung epithelial cells

Todd A. Stueckle [a,b], Yongju Lu [a], Mary E. Davis [c], Liying Wang [b], Bing-Hua Jiang [d], Ida Holaskova [e], Rosana Schafer [e], John B. Barnett [e], Yon Rojanasakul [a,*]

[a] Department of Basic Pharmaceutical Sciences, West Virginia University, Morgantown, WV 26506, USA
[b] Health Effects Laboratory Division, National Institute for Occupational Safety and Health, Morgantown, WV 26505, USA
[c] Department of Physiology, West Virginia University, Morgantown, WV 26506, USA
[d] Department of Pathology, Anatomy and Cell Biology, Thomas Jefferson University, Philadelphia, PA 19107, USA
[e] Department of Microbiology, Immunology and Cell Biology, West Virginia University, Morgantown, WV 26506, USA

ARTICLE INFO

Article history:
Received 5 December 2011
Revised 21 March 2012
Accepted 4 April 2012
Available online 13 April 2012

Keywords:
Arsenic
Lung cancer
Carcinogenesis
Global gene expression
Ingenuity Pathway Analysis

ABSTRACT

Chronic arsenic exposure remains a human health risk; however a clear mode of action to understand gene signaling-driven arsenic carcinogenesis is currently lacking. This study chronically exposed human lung epithelial BEAS-2B cells to low-dose arsenic trioxide to elucidate cancer promoting gene signaling networks associated with arsenic-transformed (B-As) cells. Following a 6 month exposure, exposed cells were assessed for enhanced cell proliferation, colony formation, invasion ability and *in vivo* tumor formation compared to control cell lines. Collected mRNA was subjected to whole genome expression microarray profiling followed by *in silico* Ingenuity Pathway Analysis (IPA) to identify lung carcinogenesis modes of action. B-As cells displayed significant increases in proliferation, colony formation and invasion ability compared to BEAS-2B cells. B-As injections into nude mice resulted in development of primary and secondary metastatic tumors. Arsenic exposure resulted in widespread up-regulation of genes associated with mitochondrial metabolism and increased reactive oxygen species protection suggesting mitochondrial dysfunction. Carcinogenic initiation via reactive oxygen species and epigenetic mechanisms was further supported by altered DNA repair, histone, and ROS-sensitive signaling. NF-κB, MAPK and *NCOR1* signaling disrupted *PPARα/δ*-mediated lipid homeostasis. A 'pro-cancer' gene signaling network identified increased survival, proliferation, inflammation, metabolism, anti-apoptosis and mobility signaling. IPA-ranked signaling networks identified altered p21, EF1α, Akt, MAPK, and NF-κB signaling networks promoting genetic disorder, altered cell cycle, cancer and changes in nucleic acid and energy metabolism. In conclusion, transformed B-As cells with their whole genome expression profile provide an *in vitro* arsenic model for future lung cancer signaling research and data for chronic arsenic exposure risk assessment.

Published by Elsevier Inc.

Introduction

Chronic arsenic (As) exposure increases lung cancer risk (Straif et al., 2009) which places it as a significant global human health hazard due to lung cancer's 12% survival rate (Payne, 2005). Inorganic As (iAs) exposures occur through domestic water supply, food consumption and inhalation via occupational or smoking activities (WHO, 2001). However, a majority of As mechanistic toxicity studies were conducted over short time periods (hours to days), with little effort placed on understanding effects of chronic (months), low dose exposures to healthy lung tissue. Currently, there is an inherent lack of understanding of both whole genome expression and signaling transduction changes associated with initiation, promotion and progression of lung cancer following chronic As exposure. Identifying and comprehending key genetic and molecular alterations during As-associated carcinogenesis will develop mechanisms of action (MOA) for human health risk assessment (Kitchin and Conolly, 2010).

As is a ubiquitous metalloid found in soil, surface water and groundwater (average 1 to 2 μg/l), but experiences increased environmental concentrations (≤3200 μg/l) due to natural or anthropogenic sources (WHO, 2001). Given that a significant percentage of drinking water sources exceed WHO recommended As guideline of 10 μg/l, continuous exposure to As contaminated water poses a threat to long-term human health worldwide. Furthermore, anthropogenic activities involving ore combustion, such as mining, coal combustion and other industrial activities release As_2O_3 into the atmosphere (ATSDR, 2007). Urban air concentrations average 0.02 to 0.03 μg inorganic As/m^3 while immediate vicinity concentrations of industrial

* Corresponding author at: PO Box 9530, Department of Basic Pharmaceutical Sciences, West Virginia University, Morgantown, WV 26506, USA. Fax: +1 304 293 2576.
E-mail addresses: tstueckle@hsc.wvu.edu (T.A. Stueckle), yongju6@hotmail.com (Y. Lu), mdavis@wvu.edu (M.E. Davis), lmw6@cdc.gov (L. Wang), bhjiang@jefferson.edu (B.-H. Jiang), iholaskova@hsc.wvu.edu (I. Holaskova), rschafer@hsc.wvu.edu (R. Schafer), jbarnett@hsc.wvu.edu (J.B. Barnett), yrojan@hsc.wvu.edu (Y. Rojanasakul).

0041-008X/$ – see front matter. Published by Elsevier Inc.
doi:10.1016/j.taap.2012.04.003

point sources range 0.1 to ≥ 50 μg/m^3. Direct occupational exposures historically range 50 to 5000 μg/m^3 (ATSDR, 2007; Offergelt et al., 1992; Smith et al., 1977). Expected tissue dose concentrations for the general public range 0.1 to 1.0 μM inorganic arsenic (Carter et al., 2003; Gentry et al., 2010). Inhaled As_2O_3-containing particles are either well absorbed or persist within the lung (ATSDR, 2007). Once in aqueous suspension As_2O_3 can transform to arsenite, a known and wide-spread carcinogen present in drinking water, experiences absorption and biotransformation by cells and persists in lung tissue (Thomas et al., 2001; Carter et al., 2003). Elevated levels of arsenicals from atmospheric, sediment and drinking water exposures potentially contribute to elevated rates of lung cancer (IARC, 2009; Putila and Guo, 2011). Long-term exposures via inhalation or dermal contact is known to increase rates of lung and skin cancer (ATSDR, 2007; Pershagen et al., 1984; Tokar et al., 2010a).

Following uptake As can experience valence alterations, biomethylation and rapid excretion from the human body primarily as monomethyl- and dimethyl-As (Carter et al., 2003; Thomas et al., 2001). Liver and kidney tissues rapidly uptake and remove As while other tissue types (e.g. lung) tend to retain total As and can convert iAs to dimethyl As (Thomas et al., 2001). Trivalent As exhibits the highest toxicity profile, however growing evidence suggests methylated As may pose greater cyto- and genotoxic risk to methylating cells (Chilakapati et al., 2010; Dopp et al., 2010; NRC, 2001; Thomas et al., 2001).

Epidemiological studies describe chronic As exposures that induce skin, urinary, liver and lung cancers (NRC, 2001), however a clear description of mode(s) of action is absent. *In vitro* and *in vivo* studies suggest that As absorption results in complex molecular interactions resulting in multiple modes of action including chromosome abnormalities, oxidative damage, increased reactive oxygen and/or nitrogen species (ROS/RNS) signaling, inflammation-driven signaling, growth factor alteration, mutagenicity, decreased DNA repair mechanisms, faulty gene expression and epigenetic mechanisms leading to a loss of control over cell proliferation signaling mechanisms (Kitchin and Conolly, 2010; Ren et al., 2011; Salnikow and Zhitkovich, 2008). Exposed cells typically exhibit altered apoptotic behavior, prolonged inflammation, activation of proliferative and carcinogenic signaling pathways that lead to neoplastic cells exhibiting cancer phenotypes, such as tumor formation and migratory/invasive ability (Gentry et al., 2010; Trouba et al., 2000; Valko et al., 2006; Wen et al., 2008).

Recent research focus has shifted towards chronic exposures to develop *in vitro* models to comprehend carcinogenic modes of action, in part due to high tolerances in adult murine *in vivo* models (Kitchin and Conolly, 2010; Tokar et al., 2010a). Chronic *in vitro* assessments have uncovered previously unidentified gene signaling patterns (Chang et al., 2010; Druwe and Vaillancourt, 2010; Gentry et al., 2010; Pi et al., 2008; Tokar et al., 2010b), but did not adequately demonstrate whole genome signal transduction pathways driving As carcinogenesis. A large need exists for improved understanding of molecular signaling pathways to further elucidate metal- and metalloid-induced carcinogenesis at environmentally relevant exposure scenarios. Whole genome expression microarray profiling coupled with large scientific knowledge base analysis can assist in identifying novel and previously unidentified gene networks involved in tumor promotion (Chilakapati et al., 2010; Ganter and Giroux, 2008; Posey et al., 2008).

This investigation's primary objective was to evaluate whether chronic, *in vitro* As exposure transforms lung epithelial cells towards a malignant phenotype and identify genetic signaling mechanisms promoting cancer using *in silico* whole genome expression profiling techniques. We hypothesized that an environmentally relevant, chronic As exposure would result in signaling pathway changes and development of functions that promote cancer behaviors in lung epithelial cells. Characterization of changes in molecular signaling mechanisms following chronic exposure will generate useful MOA data to assist human health risk assessment strategies and epidemiologic studies in addressing iAs-induced lung cancer.

Materials and methods

Cell culture procedures. Human lung bronchial epithelial cells (BEAS-2B) at 5th passage, immortalized with SV40 large T-antigen, were acquired from Dr. Fei Chen at NIOSH (Morgantown, WV). Cells were maintained in DMEM with 5% fetal bovine serum, 2 mM L-glutamine and 100 U/ml penicillin and streptomycin. Cell cultures were held in a humid, 37 °C and 5% CO_2 cell culture incubator.

As chronic exposure. To assess lung epithelium transformation during chronic As exposure, BEAS-2B cells at 10th passage were exposed to an occupational-relevant concentration of arsenic (III) oxide (Sigma Aldrich) for 6 months. Previous studies involving continuous As exposure suggested that key signaling alterations leading to malignant transformation occurs 4 to 7 months of exposure (Achanzar et al., 2002; Tokar et al., 2010b). As_2O_3 spiking solutions in sterile PBS were diluted in fresh media and added to culture plates. As_2O_3 exposed cells were referred to as B-As to distinguish them from non-passage (BEAS-2B) and passage (B-Control) control cells. Unexposed BEAS-2B cells (1×10^5 cells/well) were seeded to duplicate 6-well plates. After 24 h, cell cultures were exposed 2.5, 5, 10 and 25 μM As_2O_3 to identify a concentration resulting in long-term cell survival and at a reasonable environmental concentration (1 μM As_2O_3 = 149.85 μg/l elemental As). Spiked media was changed every 3 to 4 days while cells were passaged once every 7 days for 26 total passages. Only 2.5 μM As_2O_3 treated cells survived past Day 21 (data not shown) and were subsequently maintained for 6 months. This concentration represented a moderate occupational inhalation exposure (Carter et al., 2003; ATSDR, 2007). All treatments were passage matched and cells were not allowed to become over-confluent. Post-passage cell densities were not allowed <20% confluency for a majority of the exposure. B-As cells at 4 month exposure began to exhibit increased proliferation. Therefore, post-confluent densities of B-As cells were kept >10% for the last 6 passages to allow for adequate growth space.

Cell proliferation assays. Cells were assayed for enhanced proliferation ability over 24 to 72 h using Cyquant and MTT assay procedures. Briefly, cells were seeded (5000 cells/well) in quadruplicate in a 96-well plate in normal growth medium. Cells were incubated for 48 h and then the media was changed with 100 μl of 1× Cyquant dye solution (Invitrogen) and incubated for 1 h. Each sample's fluorescent intensity was measured at the emission (535 nm) and excitation (485 nm) wavelengths. MTT assay (Invitrogen) was performed at 24, 48 and 72 h with the same above experimental design. To ensure optimal growth conditions, cells were PBS washed and supplemented with fresh medium at 48 h. 10 μl of 12 mM MTT reagent was added to each well at each time point, incubated for 4 h, solubilized overnight and assessed for increased absorbance at 570 nM. To visually assess cell morphology and proliferation, 5×10^5 cells in 6 cm^2 dishes were seeded and observed over 72 h.

Colony formation assay. Anchorage-independent growth assessment of treatments was performed using a soft agar plate assay. Briefly, 15% FBS MEM *x*2 concentrate media with 1% gentamicin was mixed with DifCo agar in a 44 °C water bath to obtain 0.5% agar medium. BEAS 2-B, B-Control and B-As cells were suspended in agar (1×10^4 cells/well), slowly layered into an agar covered 6-well plate and allowed to solidify. Cell colonies were maintained in normal incubation conditions and observed at Day 14 for colony counts and size. Colonies were digitally imaged using an inverted Leica DMIL compound microscope fitted with a Leica DFC 490 camera and Leica Application Suite software. Colony area was determined by measuring colony border contours around 200 randomly chosen colonies per treatment using Image Pro Plus (ver.4.5) software.

Migration and invasion transwell assays. Cells in serum-free media from each treatment, at 3×10^4 and 1.5×10^4 cells/well for migration and invasion assays, respectively, were added to rehydrated inserts with 8 μm pores (BD Biosciences). Duplicate inserts were placed into wells containing 750 μl of 10% FBS media and incubated for 24 and 48 h for migration and invasion, respectively. Four experimental runs were performed. Adherent cells on the underside of a membrane were fixed and stained using Diff-Qik solution, dried overnight, digitally imaged and counted.

Animals. Nu/nu (*Crl:NU-Foxn1^{nu}*) female mice were purchased from Charles River (Wilmington, MA) at 6 weeks of age. All nude mice studies were conducted in accordance with federal and institutional animal use guidelines and followed the approved protocol ICUC #09-0402 submitted to the West Virginia University Institutional Animal Care and Use Committee. Mice were housed in filter top cages and provided sterile chow and water *ad libitum*. Mice were acclimated for 1 week prior to use in any experiment.

Cell preparation for in vivo sc injection. Non-transformed BEAS-2B and transformed B-As cells were washed and then suspended at 10^7 per ml in Glycosil/Gelin-S gel matrix. The matrix gel was prepared according to the manufacturer's (Glycosan Biosystems, Salt Lake City, UT) directions. Briefly, a 1:1:0.5 mixture of Glycosil:Gelin-S:Extralink was added to the pellet to produce sufficient cells and matrix to inject all mice in a particular experiment. A suspension of 10^6 tumor cells in 0.1 ml of gel matrix cells were injected sc on both sides of the animal using a 23 G needle and the progression of tumor development monitored over a 14 day period. Ten mice were used for each treatment group. At the end of the 14 day period, the animals were euthanized and the tumors harvested for further characterization. B-Control cells were previously tested for *in vivo* tumor formation using similar methods (Wang et al., 2011).

Tumor harvest. Tumor size was measured in two diagonal directions by using hand-held calipers and calculating volume using the equation: volume (mm^3) = [length (mm) × width $(mm)^2$]/2. At the time of tumor removal, the tumors were weighed on an analytical balance and the weight of the tumor recorded. In some animals that received the control, i.e., non-transformed BEAS-2B cells, there appeared to be a small bump that could have been tumor. However, on dissection of the area, these bumps were composed of gel matrix only and no true tumor growth was actually present. Digital photographs of the tumors in the animals were also taken at this time.

Intravenous tumor cell injection. BEAS-2B and B-As cells were injected intravenously (iv) via the retroorbital plexus (Hall et al., 2007). Five and nine animals were used for BEAS-2B and B-As injections, respectively. Animals were anesthetized by intraperitoneal (ip) injection of optimal concentrations of Ketamine-HCL (Bionichepharma, Lake Forest, IL) and xylazine (Lloyd Laboratories, Shenandoah, IA). Once anesthetized, 10^6 BEAS-2B or B-As cells in a volume of 0.1 ml isotonic injectable saline were injected by introducing a 27 G needle behind the eye into the retroorbital venous plexus. At the conclusion of the iv injection procedure, yohimbine was administered ip to counteract the anesthetics and the animal allowed to recover. Animals were euthanized at 14 days and subjected to histopathological evaluation.

Histopathology. Processing of sc tumors, head, lung, and liver samples were performed according to established necropsy and histology procedures. Briefly, tumors and organs were removed, weighed, fixed in 4% paraformaldehyde and embedded in paraffin. Tissue samples were sectioned, stained with hematoxylin and eosin and mounted onto glass slides. Stained cross-sections were evaluated for morphology and presence of tumors. All tissue slides were evaluated by a board certified pathologist.

Whole genome expression microarray analysis. Global gene expression for each treatment was determined using high-throughput mRNA microarray analysis following MIAME guidelines. B-Control (n = 4) and B-As (n = 3) cell RNA replicate samples were collected with TRIzol (Invitrogen) post-exposure. RNA quality was assessed using gel electrophoresis and 260/280 nm absorbance ratio. Samples stored at −80 °C were shipped to ArrayStar (Rockville, MD). Samples were treated with DNase digestion and analyzed for RNA quality using Nanodrop ND-100 and Bioanalyser 2100. Samples were amplified, Cy3 labeled using Agilent Quick Amp Labeling Kit and hybridized to Agilent 4x44K Whole Human Genome Oligonucleotide Microarray (#014850) in Agilent SureHyb Hybridization Chambers. One microarray replicate was performed per sample. After washing processed slides were scanned with an Agilent G2505B DNA scanner.

Agilent Feature Extraction Software (ver. 10.5.1.1) gene expression text files were imported into GeneSpring GX (ver. 10.0) for normalization using Agilent FE one-color scenarios. Only genes marked marginal or present in all samples were used (n = 20,232). Two sample *t*-tests assuming equal variance ($p \le 0.05$) with a fold-change screening ($\ge \pm 2$-fold) were used to identify differentially expressed genes (DEGs) for B-As compared to B-Control cells. Unsupervised hierarchical cluster analysis using TIGR MultiExperiment Viewer software (ver. 4.6) generated DEG heat maps. Agglomerative clustering was performed using Pearson correlation coefficient and average linkage between clusters for distance estimates. All gene expression data were deposited to NCBI's Gene Expression Omnibus and is accessible via accession number (GenBank ID: GSE33520).

Ingenuity Pathway Analysis. To reveal cancer-related gene signaling networks (GSNs) in B-As cells, Ingenuity Pathway Analysis (IPA, ver. 8.6; Redwood City, CA; www.ingenuity.com) was performed. Tab-delimited text files containing gene IDs, expression data and *t*-test p-values were uploaded into IPA. Score rankings for the top molecular/cellular functions, diseases, toxicology functions, canonical pathways and IPA-identified GSNs were calculated using IPA-generated negative logarithm p-values. P values and GSN scores reflected likelihood tests of a gene occurring in a given pathway versus other pathways based on pure chance. Top-ranked GSNs were mapped and cancer-related genes were identified. Initial evaluation of functions and networks suggested that B-As cells exhibited cancer-related gene signaling and functions. Therefore, cancer GSNs were created and mapped by filtering only those DEGs known to play a role in cancer. Lastly, cancer cells typically exhibit increased proliferation, tumor formation, migration, invasion and anti-apoptosis abilities. Cell behavior GSNs were developed for each of these phenotypes to assist in identifying signaling patterns. Genes passed the filter if they promoted the behavior and were up-regulated or antagonized the behavior and were down-regulated.

Real time polymerase chain reaction validation. Ten cancer-related DEGs were subjected to rtPCR to validate microarray gene expression data. Intron-spanning primers and probes were designed using ProbeFinder 2.45 (Roche) and obtained from Operon (Supp. Table 1). RNA sample quality were assessed using NanoDrop 1000 (Thermo Scientific), reverse transcribed, and amplified using 2720 Thermo Cycler (Applied Biosystems) in triplicate. Quantitative rtPCR was conducted on an ABI 7500. Each thermocycling reaction used 25 μl total volume containing 7.25 μl cDNA, 2.5 μl primers and 12.5 μl Roche Taqman Master Mix. Relative expression levels to GAPDH were determined using $2^{-\Delta\Delta ct}$ and compared to microarray values using a *t*-test.

Statistical analyses. All cell behavior data were analyzed using one- or two-way ANOVA to compare across treatment groups ($\alpha = 0.05$). Tumor volumes and weights were compared across treatment groups using a two-way ANOVA. A post-hoc Tukey–Kramer HSD was conducted to identify significantly different treatment groups. *In vivo* tumor incidence data were analyzed using Fisher's exact test

($\alpha = 0.05$). Two-tailed *t*-tests ($\alpha = 0.05$) were used to compare rtPCR to microarray expression fold change values for each gene in the microarray validation analysis. All statistical analyses were performed using JMP SAS 8.0.

Results

B-As cells exhibit enhanced proliferation, colony formation, and invasion abilities

Since cancer cells typically exhibit uncontrolled cell growth, tumor formation and tissue invasion abilities, BEAS-2B cells chronically exposed to 2.5 μM As_2O_3 were assessed for a malignant phenotype using several *in vitro* cell behavior assays. To ascertain whether B-As possessed enhanced proliferation ability, control and B-As cell proliferation were assayed using Cyquant and MTT methods. Cells were seeded in 96 well plates and assayed for cell number and proliferation between 24 and 72 h. B-As exhibited significant increase in cell number at 48 h ($F = 224.8$, $p < 0.001$) compared to both controls (Fig. 1A). Chronic As exposure's effect on cell proliferation depended on time (Fig. 1B; $F = 5.59$, $p = 0.0002$). At 24 h, B-As cell proliferation had doubled while at 72 h, it had more than tripled compared to controls. B-Control cells possessed a significantly lower mitochondrial metabolic rate than BEAS-2B cells for the first 48 h. Visual observation of cultured cell types over 72 h resulted in B-Control cells showing low growth, slender morphology with long pseudopodia typical of BEAS-2B cells. Conversely, B-As cells exhibited increased proliferation and cobblestone cell morphology (Fig. 1C). Both proliferation assays and visual observation indicated that B-As cells possessed a transformed, accelerated growth phenotype.

To assess whether B-As cell exhibited anchorage-independent growth, both control and As-exposed cells were assayed for soft agar colony formation ability. Cells were suspended in solidified soft agar and cultured for 14 days. All three cell types significantly differed from each other in their colony formation ability (Fig. 2A; Supp. Fig. 1; $F = 227.6$, $p < 0.001$). B-Control and B-As cells exhibited 5.1- and 6.9-fold greater colony formation ability than BEAS-2B cells, respectively. B-As cells displayed a significant 1.4-fold increase in colony formation capacity compared to B-Control cells ($p < 0.05$). Although both passaged cell lines exhibited increased number of colonies, B-As cells displayed significantly greater colony size than both BEAS-2B and B-Control cells ($F = 90.9$, $p < 0.0001$) indicating an accelerated colony proliferation capacity.

Cancer cells typically exhibit increased cell mobility and invasion of neighboring tissues, even in nutrient deprived conditions. To ascertain if B-As cells possessed greater invasive behavior compared to controls, cells were subjected to transwell, chemotaxis assays in serum-free media. B-As cells exhibited significantly greater migration ($F = 37.4$, $p < 0.001$) and invasion ability ($F = 89.2$, $p < 0.001$) in serum-free media than both control cell lines (Fig. 2B). Collectively, B-As cells exhibited transformed phenotype characterized by enhanced proliferation, colony formation, migration and invasion abilities typical of cancer cell-like behavior.

B-As cells form in vivo tumor and lung metastases

To determine whether the *in vitro* transformed B-As cells possessed a malignant phenotype, BEAS-2B and B-As cells were suspended in matrix gel and sc injected into Nu/nu mice. Tumor incidence, volume and mass were assessed 14 days post-injection. B-As cells showed 80% *in vivo* tumor formation incidence 14 days post-injection which was significantly greater than injected BEAS-2B cells (Fig. 3A, top; $\chi^2 = 16.9$, $p < 0.0001$). The effect of As exposure on tumor volume depended on time (Fig. 3A, middle; $F = 3.54$, $p = 0.048$). Specifically, B-As tumor volume doubled between 7 and 14 days post-injection while BEAS-2B volume decreased over time. In a separate related study,

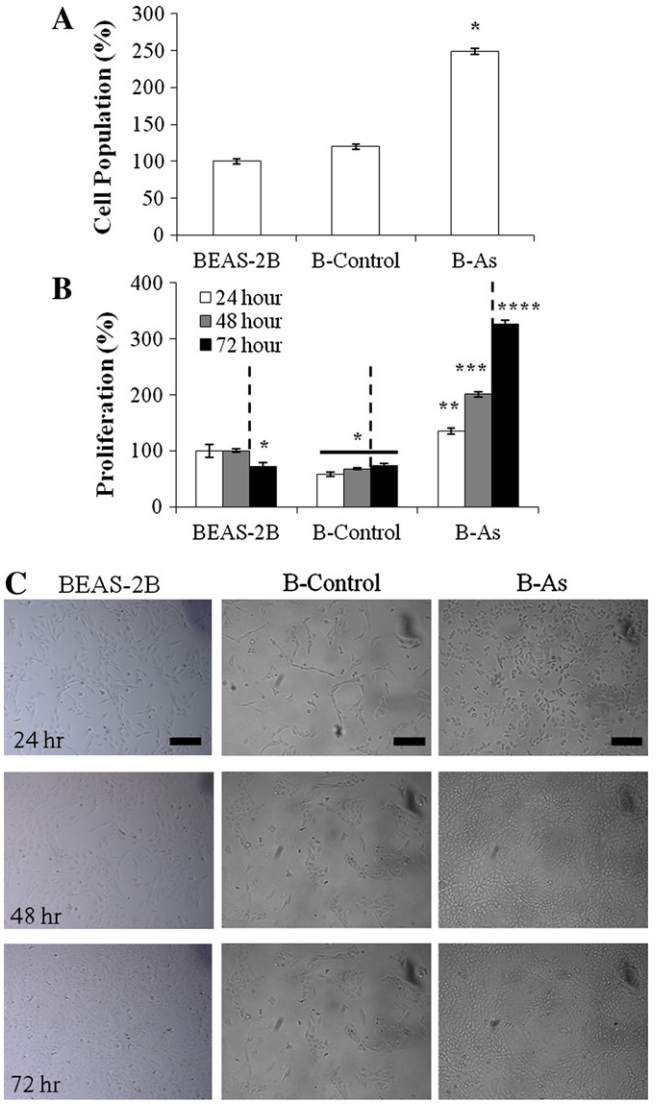

Fig. 1. Enhanced cell proliferation in chronic arsenic-exposed lung epithelial cells. A, B-As cells exhibited a significant increase in cell population at 48 h assayed by Cyquant. B, B-As cells displayed a significant time-dependent increase in cell proliferation in MTT assay compared to control cell lines (24–72 h). Dashed lines indicates a media change. Data represent Mean ± SE ($n = 4$). Different * indicate significantly different treatments compared to each other and BEAS-2B cells ($p < 0.05$). C, B-As cells (right) displayed rounded cell morphology and rapid cell proliferation while BEAS-2B (left) and passage matched control cells (B-Control; center) displayed normal morphology and growth. Bars = 200 μm.

sc injected B-Control cells displayed low tumor volume at 10 days and disappeared by 14 days (Wang et al., 2011). In addition, B-As tumors exhibited significantly greater mass versus non-existent BEAS-2B cell tumors at 14 days (Fig. 3A, bottom; $F = 103.6$, $p < 0.0001$). Histological sections of B-As sc tumors revealed large, multinucleated cells with cancer cell morphology (Fig. 3B; Ullmann et al., 2003). Dissection of two flat masses in BEAS-2B injected mice revealed only gel matrix with no tumors present. These results indicated that B-As cells represent a malignant, transformed phenotype following chronic As exposure.

Next, cells were retroorbitally (ro) injected into mice to evaluate B-As cell metastatic ability. B-As cells exhibited significantly greater tumor incidence at 14 days post-injection than BEAS-2B cells in forming both periorbital/parasinal tumors and lung metastases (Table 1; $p < 0.05$). Specifically, all mice ro injected with B-As cells formed large head tumors characterized as periorbital abscesses possessing some acute inflammatory infiltrate (data not shown). Two-thirds of B-As

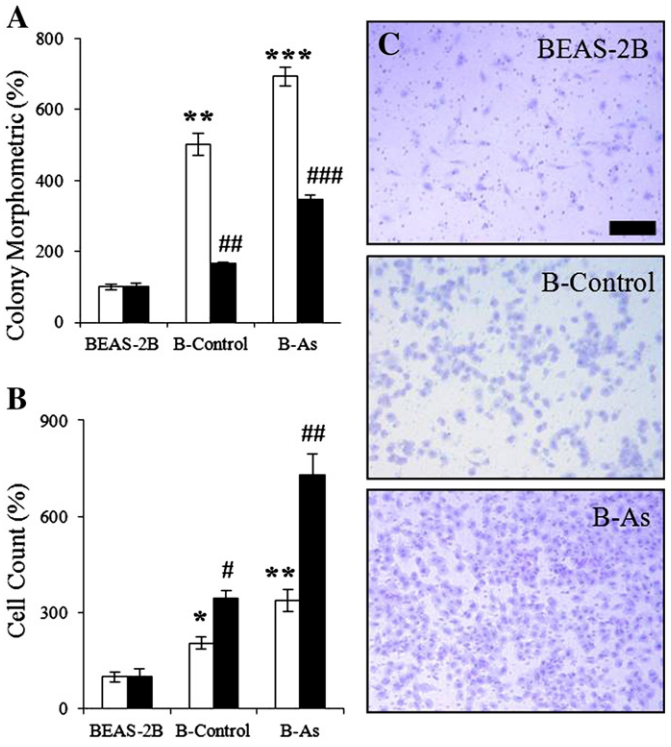

Fig. 2. Enhanced colony formation and invasion/migration phenotype of chronic arsenic-exposed lung epithelial cells (B-As) compared to control cell lines. A, Passage control (B-Control) and B-As cells displayed a significant increase in the number of colonies formed (white bars) and colony size (black bars) after 14 days compared to BEAS-2B. B, B-Control and B-As cells displayed a significant increase in migration (white bars) and invasion (black bars) ability over BEAS-2B cells. Data represent Mean ± SE (n = 3–5). Different * and # indicate significantly different treatments compared to each other and BEAS-2B cells ($p<0.05$). C, Increased invasion ability of B-As cells in a transwell Matrigel assay; bar = 200 μm.

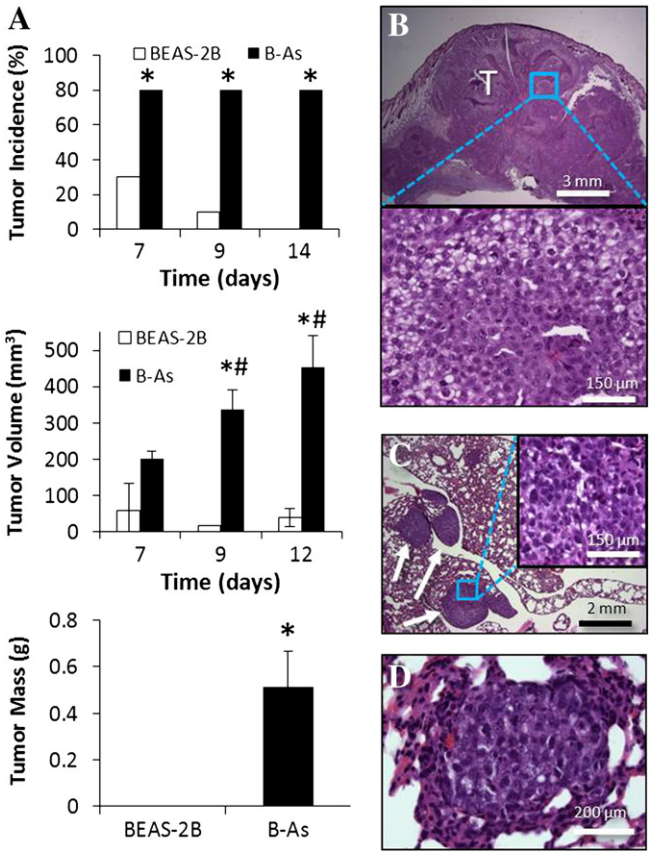

Fig. 3. *In vivo* tumor formation of injected B-As cells into Nu/nu female mice. A, B-As cells showed significant increase in sc tumor incidence (top), tumor volume (middle) and tumor mass (bottom) compared to BEAS-2B cells. Data represent Mean ± SD (n = 10). * represent treatments significantly different from controls while # signifies treatments significantly different from 7 days ($p<0.05$). B, Histopathology of a large sc B-As cell tumor (top) at 14 days post-injection containing multi-nucleated cells (bottom). 'T' indicates tumor tissue. C, Retroorbital injections of B-As cells resulted in miliary and nodular metastatic lung tumors within alveolar and interstitial tissues at 14 days. White arrows indicate secondary tumors. D, Small nodular metastatic tumor.

injected mice developed lung metastases with miliary (Fig. 3C) and nodular appearance (Fig. 3D) associated with small airway and interstitial tissue (Supp. Fig. 2). No liver metastases were found for either B-As nor BEAS-2B cells.

B-As cell genome experienced changes in cellular/molecular functions commonly associated with cancer

To assess arsenic-mediated carcinogenic MOAs and gene signaling networks promoting lung cancer, we performed cDNA hybridization and whole genome expression analyses on mRNA collected from human BEAS-2B lung epithelial cells chronically exposed to arsenic trioxide. A *t*-test and 2-fold change filtering of expression data resulted in 1373 up- and 585 down-regulated DEGs in B-As cells. 70.2% of B-As DEGs was skewed towards over-expression while 69.3% was within ±2 to 4-fold change (Fig. 4A). Hierarchical cluster analysis revealed clear differences in gene expression between the two treatments. Several large clusters of genes with common over- and under-expression were evident in B-As compared to B-Control cells (Fig. 4B).

To identify arsenic-induced alterations of cellular, disease and toxicology functions, IPA analysis was used to evaluate DEG microarray data using current scientific literature. Chronic As exposure resulted in significant cellular function changes associated with cell assembly/organization, cell cycle, cell morphology and cell death (Fig. 4C). Top-ranked molecular function changes were associated with lipid metabolism, nucleic acid metabolism and small molecule biochemistry. A large number of DEGs involved in cell death, cell growth and differentiation, lipid metabolism, small molecule biochemistry and protein synthesis were identified in B-As cells. Evaluation of top-ranked diseases resulted in cancer and genetic disorder as first and third ranked diseases, respectively (Table 2). B-As cells displayed significant toxicological responses associated with mitochondrial processes, fatty acid metabolism, *PPARα* signaling, inflammation and oxidative stress. Common to these top toxicological functions included over-expressed Phase II detoxification enzymes (*GSTμ*), fatty acid metabolism enzymes and genes associated with *PPARα* down-regulation. In summary, categorization of DEGs into

Table 1
Tumor incidence and diameter data from retroorbital injections of BEAS-2B and B-As cells in Nu/nu female mice.

Treatment	Positive cases	N	Tumor incidence (%)	Fisher exact p-value[a,b]	Greatest dimension (mm; X, ±SD)
Periorbital/parasinal tumors					
BEAS-2B	0	5	0	–	0
B-As	9	9	100	0.0005*	3.7, 0.65
Lung metastases					
BEAS-2B	0	5	0	–	0
B-As	6	9	67	0.03*	0.52, 0.10
Liver metastases					
BEAS-2B	0	9	0	–	0
B-As	0	5	0	NSD	0

[a] Stars and NSD indicate a significant or no significant difference compared to BEAS-2B control, respectively.
[b] Dashes represent control group.

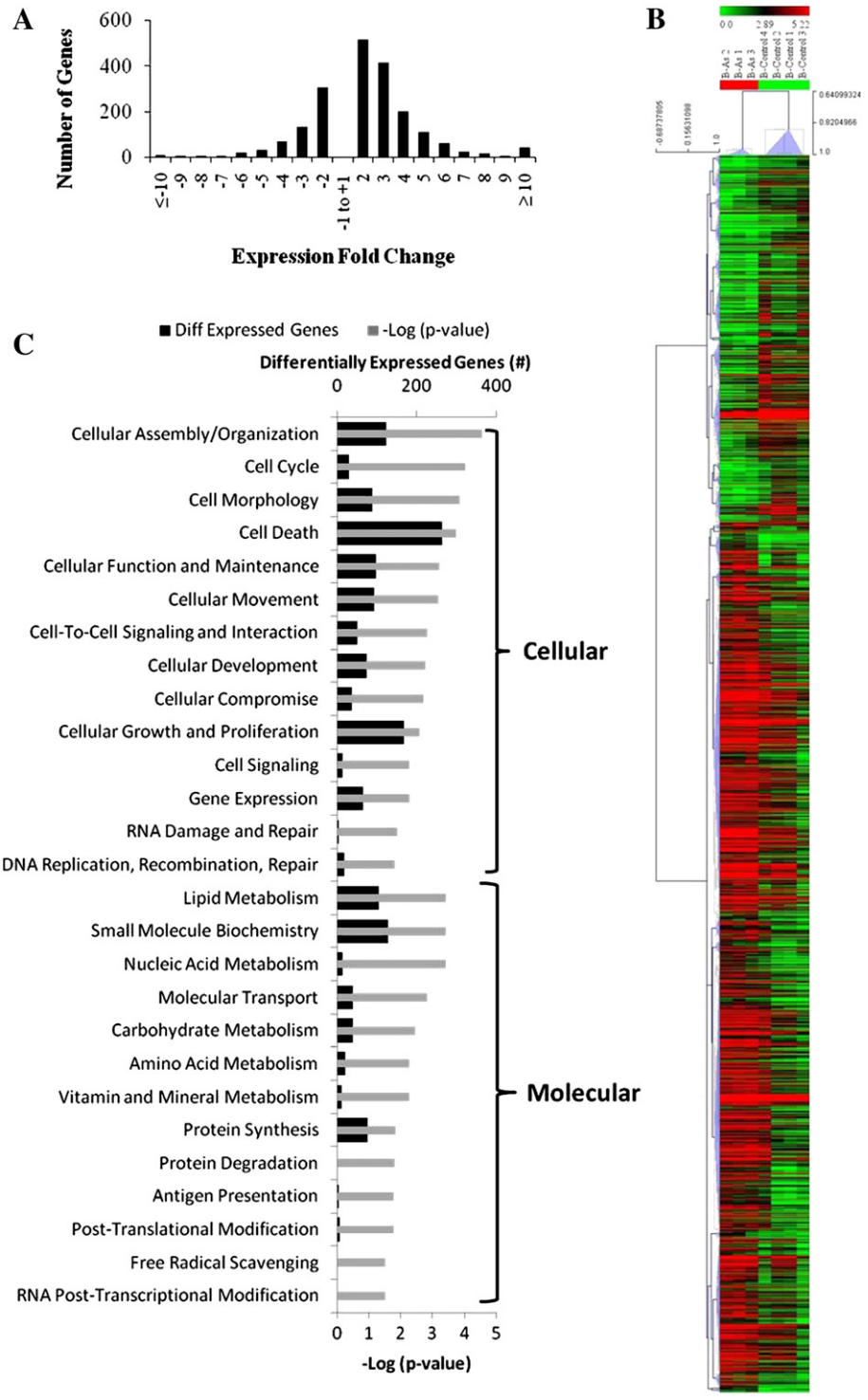

Fig. 4. Altered gene expression profile and cellular/molecular functions in chronic As-exposed lung epithelial cells (B-As) compared to passage control cells. A, Distribution and B, hierarchical cluster analysis of differentially expressed genes (DEGs) in B-As cells revealed distinct clusters of over- or under-expressed DEGs. C, Highest ranked cellular and molecular biofunctions of B-As cells determined by Ingenuity Pathway Analysis.

cellular and disease functions suggested that B-As cells experienced gene expression changes in functions commonly associated with malignant cells.

Chronic As exposure disrupted mitochondrial function and PPARα/δ homeostasis in BEAS-2B cells

To further elucidate alterations to mitochondrial function and *PPARα* signaling, an in-depth analysis of related canonical pathways was performed in IPA. Investigation of significantly altered B-As cell canonical pathways indicated that valine, leucine and isoleucine degradation, propanoate metabolism and pyruvate metabolism pathways experienced the most significant changes. The remaining top 20 pathways primarily centered on mitochondrial function, energy metabolism and protein metabolism (Supp. Table 2). A significant percentage of DEGs in mitochondrial metabolism pathways experienced up-regulation suggesting increased metabolic energy output. Although pyruvate dehydrogenase kinase (*PDK1*) up-regulation indicated pyruvate

Table 2
Top-ranked disease and toxicology functions in chronic arsenic (III) oxide-exposed BEAS-2B cells.

Function	p-value[a]	Diff. expressed genes in pathway[b]
Diseases		
Cancer	3.34E-06	321
Gastrointestinal disease	3.34E-06	104
Genetic disorder	3.34E-06	647
Neurological disease	1.44E-04	392
Reproductive system disease	3.99E-04	155
Toxicology		
Mitochondrial dysfunction	3.08E-04	21/125
LPS/IL-1 mediated inhibition of RXR function	1.30E-03	26/187
Fatty acid metabolism	7.06E-03	18/130
Mechanism of gene regulation by peroxisome proliferators via PPARα	2.20E-02	13/95
Oxidative stress	5.67E-02	8/57

[a] Significance value of differentially expressed genes compared to untreated controls.
[b] Indicates number of differentially expressed genes in each function compared to total genes in the pathway.

shuttling towards anaerobic respiration, all five major mitochondrial electron transport chain complexes possessed up-regulated DEGs (Table 3), suggesting an increase in energetic output. Further investigation of DEGs associated with mitochondrial dysfunction and *PPARα* signaling revealed evidence for pro-cancer alterations. Increased ROS-induced stress was evident in the mitochondrial dysfunction pathway with up-regulation of several pro-oxidative stress (*MAOA*, *GPD2*, *PDHA 1/2*, *COX* family) and oxidative stress protective (*SOD2*, *PRX3*) genes. Down-regulation of *PPARα* and *PPARδ* via up-regulation of Src/MAPK, NF-κB, and *NCOR1* signaling suggested dysfunctional lipid homeostasis and altered energy metabolism (Fig. 5). These results indicate that chronic arsenic exposure increased mitochondrial metabolism, ROS signaling potential and *PPARα/δ*-controlled energy expenditure, thereby affecting B-As cell proliferation.

Top over- and under-expressed genes reveal B-As cell dysregulated gene signaling

Identification of the top most up- and down-regulated genes uncovered evidence for dysregulated gene signaling controlling cell proliferation, cell cycle, inflammation, apoptosis and cytoskeleton functions (Supp. Table 3). B-As cells displayed over-expressed inflammatory genes (*IL1A*, *CXCL5*) and known pro-cancer markers for malignant carcinomas (*AGR2*, *LCP1*, *TM4SF1*). Down-regulated genes played roles primarily in promoting or inhibiting cell growth/proliferation (*SULF2*, *IL4R*, *CDK11B*, *TGFBR2*). Seven of the twenty most DEGs were present in the B-As pro-cancer behavior GSN (described below) while an additional seven genes presided in GSNs associated with cancer cell behavior, such as pro-proliferation and anti-apoptosis.

Gene signaling network analysis reveals cancer-associated signaling in B-As cells

Based on IPA's canonical pathway and disease evidence, B-As cancer GSNs and IPA top-ranked GSNs were evaluated to identify potential cancer signaling networks. DEGs were filtered based on known involvement in cancer signaling. 321 cancer-associated genes were identified with 167 genes with known signaling interactions were placed into a B-As cancer GSN (Supp. Fig. 3). Pro- and anti-cancer signaling was evidently centered on 11 up-regulated (*EGFR*, *PTEN*, *SHC1*, *CAV1*, *RHOA*, *GSK3β*, *CDKN1A*, *CYCS*, *IL1A*, *NRG1*, *IL15*) and 8 down-regulated (*FGF2*, *BCAR1*, *EGR1*, *JUN*, *FOXO3*, *PLCG1*, *TNFSF10*, *HTT*) signaling hub genes. Biofunctions associated with the B-As cancer network centered on cellular growth and proliferation, cell death, and cell cycle. Of these genes, 140 genes were identified as promoting cancer with 58 genes with known interactions placed into a B-As pro-cancer GSN (Fig. 6A). The B-As pro-cancer GSN possessed the signaling hub genes *EGFR*, *IL1A*, *IL15*, *FGF2*, *JUN*, *NRG1*, *PTEN* and *TNFSF10*. Four cytokine genes (*IL1A*, *IL15*, *NRG1*, *FGF2*) potentially drove downstream pro-cancer signaling including up-regulation of *EGFR*, *PTEN*, *SOD2* and *CHUK* and down-regulation of *JUN*, *EGR1*, *IRF1*, *TNFSF10*, *TGFBR2* and several metallothioneins. For unconnected pro-cancer genes, DEGs associated with glutathione S-transferases, lipid and protein metabolism, mitochondrial metabolism, cellular structure and cell signaling were observed (Supp. Table 4). Of note, 7 different metallothioneins were all down-regulated. Nineteen and seven DNA recombination and repair genes were up- and down-regulated, respectively, while 15 of these genes occurred in the B-As cancer GSN (Supp. Table 5). Also, 6 out of 20 DEGs associated with histone H1, H3 and H4 structure and epigenetic modification were identified as

Table 3
Differentially expressed genes in the B-As mitochondrial dysfunction canonical pathway.

Gene symbol	Fold change	Entrez gene name	Entrez gene function
ATP5B	4.51	ATP synthase, H+ transporting, mitochondrial F1β	Complex V, mitochondrial ATP synthesis
ATP5C1	3.78	ATP synthase, H+ transporting, mitochondrial F1γ	Complex V, mitochondrial ATP synthesis
BACE1	−2.74	Beta-site APP-cleaving enzyme 1	Proteolytic processing of APP
COX11	2.79	COX11 cytochrome *c* oxidase assembly homolog	Complex IV, cytochrome *c* electron transfer
COX15	4.01	COX15 homolog, cytochrome *c* oxidase assembly	Complex IV, cytochrome *c* electron transfer
COX10	4.72	COX10 homolog, cytochrome *c* oxidase assembly	Complex IV, cytochrome *c* electron transfer
COX5A	2.99	Cytochrome *c* oxidase subunit Va	Complex IV, cytochrome *c* electron transfer
CPT1A	2.35	Carnitine palmitoyltransferase 1A	Long-chain fatty acid transport, mitochondria
CPT1B	−2.41	Carnitine palmitoyltransferase 1B	Long-chain fatty acid transport, mitochondria
CYC1	2.22	Cytochrome *c*-1	Mitochondrial electron transport
CYCS	2.81	Cytochrome *c*, somatic	Mitochondrial electron transport
GPD2	2.45	Glycerol-3-phosphate dehydrogenase 2	Glycolysis, glycerol phosphate shuttle
HTRA2	2.23	HtrA serine peptidase 2	Apoptosis, MAPK14 and b-casein binding
MAOA	6.11	Monoamine oxidase A	Oxidative deamination of neurotransmitters
NDUFA10	5.53	NADH dehydrogenase 1 alpha subcomplex, 10	Complex I, mitochondrial electron transport
NDUFA9	3.42	NADH dehydrogenase 1 alpha subcomplex, 9	Complex I subunit, mitochondria
NDUFAB1	2.27	NADH dehydrogenase 1, alpha/beta 1	Complex I, electron transport, fatty acid transport
NDUFAF1	3.29	NADH dehydrogenase 1 alpha, assembly factor 1	Chaperone, Complex I, mitochondria
NDUFS1	3.31	NADH dehydrogenase Fe–S protein 1	Complex I, mitochondrial electron transport
NDUFS2	4.35	NADH dehydrogenase Fe–S protein 2	Complex I, mitochondrial electron transport
PDHA1	2.39	Pyruvate dehydrogenase alpha 1	Glycolysis, tricarboxylic acid cycle
PRDX3	6.1	Peroxiredoxin 3	Antioxidant, regulates NF-κB activation
SDHC	3.43	Succinate dehydrogenase complex, subunit C	Complex II, mitochondrial electron transport
SOD2	4.62	Superoxide dismutase 2, mitochondrial	Superoxide scavenger, hydrogen peroxide production
UQCRC2	2.79	Ubiquinol–cytochrome *c* reductase core II	Complex III, mitochondrial electron transport

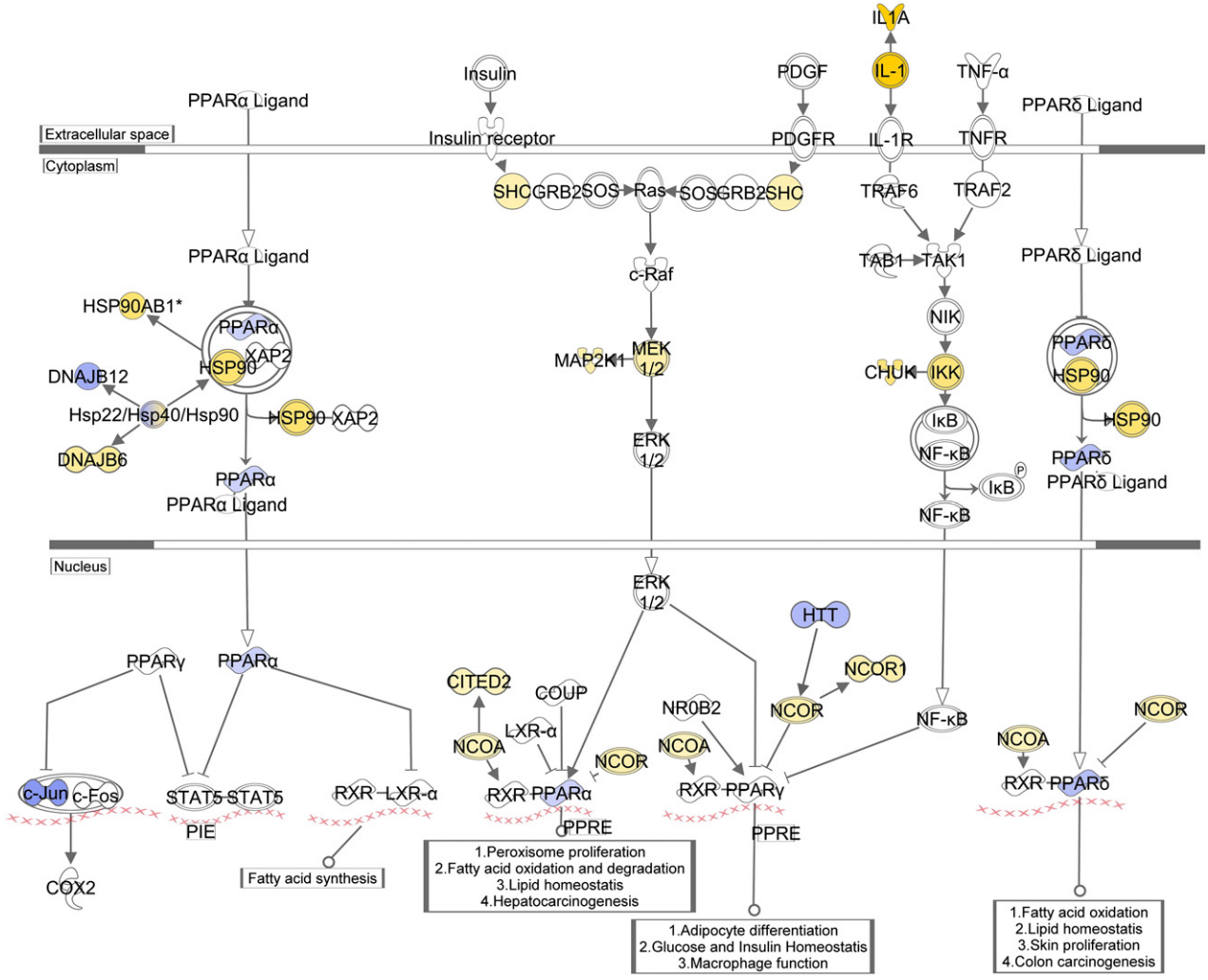

Fig. 5. *PPARα* signaling canonical pathway in chronic arsenic-exposed lung epithelial cells. Src/MAPK, NF-κB and *NCOR1* signaling appeared to disrupt *PPARα/δ* lipid homeostatic control. Yellow and blue represent up- and down-regulation, respectively, compared to unexposed controls. Color intensity signifies fold change.

pro-cancer genes (Supp. Table 6). In summary, identification of DEGs and their role in a cancer-promoting GSN indicates that B-As cells experienced several changes to established oncogenic signaling pathways.

To further identify GSNs potentially promoting a cancer phenotype, IPA was used to rank GSNs based on known gene signaling associations and likelihood tests of a given gene appearing in a given network. Top-ranked B-As GSNs involved biofunctions including gene expression/disorder, cell cycle, cancer and changes in nucleic acid and energy metabolism (Table 4). Network 1 details the up-regulation of p21 (*CDKN1A*) with downstream up-regulation of *CKS1B* suggesting cell cycle arrest in G1 phase, a common mechanism in aggressive cancers (Fig. 6B). Network 2 centered on *PLCG1*, *EEF1A1* and *ANXA2* detailing changes in tubulin metabolism, NF-κB signaling, cell adhesion and loss of Ras/MAPK negative regulatory ability (Fig. 6C). Network 3 (not shown) detailed over-expression of known tumor enhancers and suppressors of Akt activity (i.e. *AKTIP*, *TPD52*, *PTPRJ*). Networks 4 to 9 (not shown) displayed changes including altered Akt, mitochondrial ATP synthase, protein metabolism, MAPK, *PTEN*, *HTT*, *NPM1*, *FOXO3*, actin and *JUN* signaling.

To identify genes promoting specific cancer cell behaviors, DEGs were filtered for their known abilities to promote one of seven cancer cell behaviors (i.e. pro-proliferation) and subsequently mapped in a cancer cell behavior GSN. By generating seven cancer cell behavior GSNs, several genes appeared to play a key role in B-As neoplastic cell behavior (Supp. Table 7; networks not shown). Many gene signaling relationships observed in B-As pro-cancer GSN were reoccurring in the cancer cell behavior GSNs. Fifty seven genes were present in ≥3 cell behavior GSNs known to promote cancer cell behavior. Genes that occurred in a majority of these networks were *ANXA1*, *BCR*, *CAV1*, *EGFR*, *IL1A*, *IL15*, *JUN*, *MAP2K1*, *NRG1*, *RHOA*, *SHC1*, *SOD2* and *TGFBR2*. By examining ranked and cancer-associated behavior GSNs, genes commonly associated with promoting cancer through proliferation, inflammation and cell mobility were identified.

rtPCR validation of microarray data confirms several cancer-promoting genes in B-As cells

To validate our microarray expression analysis, we conducted quantitative rtPCR on ten genes associated with pro-cancer function in B-As cells compared to B-Control cells. rtPCR validation of microarray expression values confirmed the expression of genes in the B-As cancer GSN (Fig. 7). rtPCR expression values for all genes, except *CLU*, did not significantly differ from microarray values ($p > 0.05$). *JUN* and *SDC2* microarray expression were highly variable amongst replicates but were both differentially down-regulated.

Discussion

Chronic 2.5 μM As_2O_3 exposure to BEAS-2B cells resulted in cells displaying increased proliferation, migration, invasion, colony and

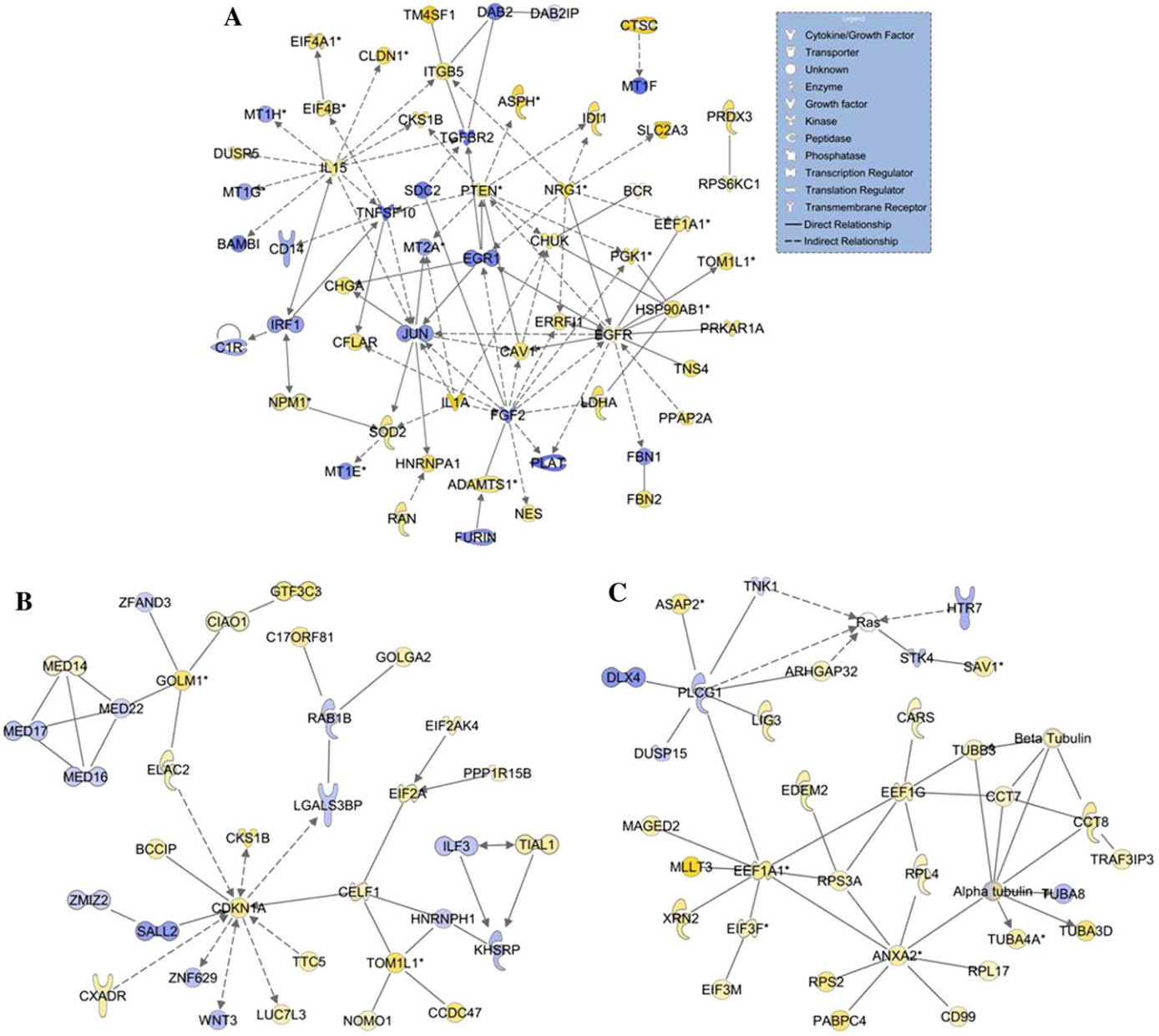

Fig. 6. Cancer gene signaling networks (GSNs) in chronic arsenic-exposed lung epithelial cells identified by IPA. A, Pro-cancer GSN of 45 genes contained signaling pathways driving proliferation, inflammation, anti-apoptosis and integrin signaling. B, Top two ranked gene signaling networks centered on p21 (*CDKN1A*) and *CKS1B* over-expression and C, EF-1A, phospholipase C and Ras/MAPK controlling kinases. Yellow and blue represent up- and down-regulation, respectively, compared to passage control cells. Color intensity signifies fold change.

tumor formation abilities accompanied by significant cancer-associated GSN alterations suggesting neoplastic transformation towards a malignant phenotype. IPA identified DEGs in a large B-As 'cancer' GSN associated with cellular organization, death and proliferation, thus suggesting the complexity of As-associated neoplastic gene signaling alterations. Evidence for mitochondrial dysfunction, ROS generation, DNA damage, inflammation, lipid homeostasis disruption and cell signaling changes supports a pro-inflammatory and ROS signaling-mediated MOA leading to overall genetic disorder, loss of cellular homeostasis and progression to a cancer phenotype.

B-As cell *in vitro*/*in vivo* malignant phenotype and GSNs agreed with recent chronic As exposure studies (0.1 to 10 μM) that report oxidative stress, protein toxicity, inflammation and increased cell proliferation leading to altered gene expression associated with cell cycle control, DNA repair and apoptosis (Chilakapati et al., 2010; Gentry et al., 2010). Chronic, low dose exposure to urinary cells and keratinocytes caused increased invasiveness, breakdown of ECM, altered cytokeratin production and *in vitro*/*in vivo* tumor formation (Pi et al., 2008; Tokar et al., 2010b). Sodium arsenite transformed murine fibroblast and small airway epithelial cells displayed similar proliferation and invasive potential with changes in Ras/MAPK, eFos/Jun, p53, phospho-RTK and NF-κB pathways (Chang et al., 2010; Trouba et al., 2000; Wen et al., 2008; 2010). Conversely, As-exposed unattached prostate epithelial stem cells displayed an aggressive, cancer stem cell phenotype due to altered developmental gene and loss of *PTEN* expression while attached cells displayed less malignant properties (Tokar et al., 2010b). Given that B-As cells exhibited similar cancer phenotype behavior to previous studies, whole genome expression profiling and *in silico* gene signaling pathway analysis provided a useful *in vitro* model to identify malignant conversion MOA for chronic As_2O_3 exposure.

Increased soft agar colony formation and migration/invasion ability in passaged B-Control versus BEAS-2B cells suggests that long term

Table 4
Top-ranked 20 significantly altered gene signaling networks in transformed B-As cells with respective hub genes determined by Ingenuity Pathway Analysis.

Hub genes[a,b]	Signaling network	Score
CDKN1A ↑, GOLM ↑	Gene expression, cell cycle, cell signaling	44
PLCG1 ↓, EEF1A1 ↑, ANXA2 ↑	Protein synthesis, RNA damage and repair, cancer	38
AKTIP ↑, Akt, KIAA1377 ↑	Cellular assembly and organization, hair and skin development and function, organ morphology	37
SMARCA4 ↑, NKX2-5 ↓, ATPases↕, peptidase ↕	Energy production, nucleic acid metabolism, small molecule biochemistry	36
PTEN ↑, RNA polymerase ↑, MAPK activity↕	Cell cycle, developmental disorder, genetic disorder	34
HTT ↓, NADH2 dehydrogenases ↑	Genetic disorder, metabolic disease, cardiovascular system development and function	34
Ap1 ↓, Actin ↑, Arp 2/3 ↕	Cellular assembly and organization, cellular function and maintenance, cellular movement	30
SMARCC ↓, Cyclin E, RNF2 ↑	Cell cycle, gene expression, cell death	30
JUN ↓, SOD2 ↑, Snare ↓	Cell death, liver necrosis/cell death, gene expression	28
MAP3K↓, p38 MAPK, CHUK↑	Gene expression, amino acid metabolism, post-translational modification	26
APBB1↑, Frizzled ↕	Tissue development, organismal development, behavior	26
PDGF BB complex, Insulin complex	Metabolic disease, genetic disorder, amino acid metabolism	26
Hsp 70/90 ↑, TSC22D1↑, 19s proteosome ↑	Post-translational modification, protein folding, carbohydrate metabolism	26
ERK↑, GNRH1↑, CHGA ↑	Cellular function and maintenance, cellular movement, nervous system development and function	25
EGFR↑, MYO5A ↑	Cellular assembly and organization, connective tissue disorders, genetic disorder	25
IL15↑, STAT4 ↑, IRF1↓	Cell death, cell cycle, hematological system development and function	25
PPARA↓, NF-κB complex	Lipid metabolism, small molecule biochemistry, amino acid metabolism	24
APOE ↓, MAPK6 ↑, COX subunits ↑	Lipid metabolism, molecular transport, small molecule biochemistry	23
IL1 ↑, FGF2 ↓, TIMP2↓, Mmp ↓	Cardiovascular system development and function, cellular movement, embryonic development	23
FSH complex, hCG complex, PXR ligand-RXR	Drug metabolism, endocrine system development and function, lipid metabolism	22

[a] All caps represent individual genes while lower case represent gene complexes and/or groups.
[b] Arrows indicate direction of differential expression. Absence of an arrow signifies no differential expression change.

passage of BEAS-2B cells can result in a transformed phenotype. A lower mitochondrial metabolic rate in B-Control than BEAS-2B cells with no difference in cell number indicates that B-Control transformation did not exhibit increased proliferation, a typical attribute of neoplastic transformation. BEAS-2B cells originated from non-cancerous lung tissue and immortalized with SV40 large T-antigen which has resulted in a mutated p53 (Gerwin et al., 1992). A weakened p53 response may partially explain the B-Control transformed phenotype. In addition, use of different culture medium from the ATCC recommended medium potentially contributed to B-Control cell's capacity for colony formation. However, recent metal and nanomaterial carcinogenesis studies using BEAS-2B cells in subchronic exposures reported soft agar colony formation in passage controls using the same medium as this study (Sun et al., 2011) but found no tumor formation following sc injection (Wang et al., 2011). American Type Culture Collection claims that BEAS-2B cells form soft agar colonies, but are non-tumorigenic in mice. At present, it is unclear how a weakened p53 affected arsenic's transformation ability and must be taken into consideration in data interpretation. Increasing evidence suggests that genetic background and other environmental factors (e.g. viral infections) may predispose cells to arsenic toxicity, thus affecting carcinogenesis and disease outcome (reviewed by States et al., 2011). At present, it is not clear whether B-As cells represent an As-induced malignant transformation, an As-enhanced transformation or whether initial As exposure altered key genetic features followed by a natural progression of cancer. Nonetheless, chronic *in vitro* arsenic exposure did further enhance and promote BEAS-2B cell transformation ability resulting in a transformed, malignant lung epithelial cell phenotype suitable for whole genome expression profiling to identify cancer-related gene signaling mechanisms.

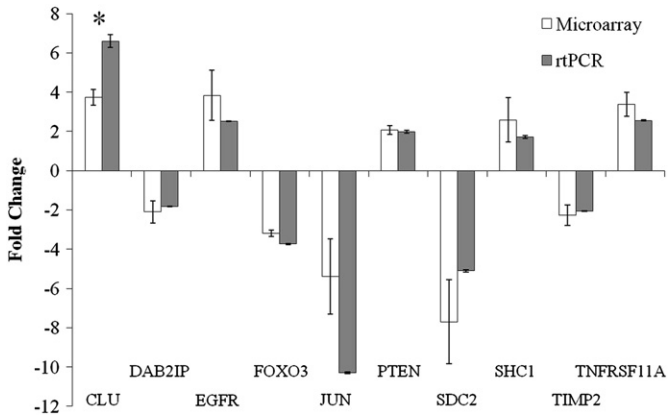

Fig. 7. rtPCR validation of Agilent microarray expression data using select genes from chronic arsenic-exposed BEAS-2B cells. Isolated mRNA was reverse-transcribed and subjected to rtPCR reaction with Roche Taqman probes. Data represent Mean ± SE, n = 3. * represents p-value < 0.05.

Pathway analysis identified potential mitochondrial oxidative stress and large scale alterations in mitochondrial small molecule biochemistry associated with increased energy production in B-As cells. Widespread gene up-regulation in each mitochondrial electron transport chain complex and increased cell proliferation suggests increased mitochondrial energy production. As_2O_3 is an established, viable cancer therapy because it targets mitochondria membrane potential disruption, cytochrome *c* release and increased ROS production (Bustamante et al., 2005). However, chronic As exposure results in tumors with altered cell signaling that promotes accelerated cell proliferation (Trouba et al., 2000; Wen et al., 2008) and oxidative damage to mitochondrial DNA that promotes carcinogenesis (Valko et al., 2006). Our results further implicate chronic As exposure targeting mitochondrial function, thus promoting ROS generation and signaling associated with cancer.

B-As cells adapted to prolonged, As-induced mitochondrial ROS generation through several ROS defense mechanisms. Aerobic respiration via oxidative phosphorylation involves decoupling of mitochondrial electron transport and superoxide ion generation during splitting of molecular oxygen (Inoue et al., 2003). Increased mitochondrial energy output along with up-regulated ROS-generating (*MAOA*, *GPD2*, *PDHA*, complexes I/IV) and ROS protective (*SOD2*, *PDX3*, *GSTμ*, *GCLC*) genes indicate increased ROS production. Given that over-expressed *SOD2* is an adaptive mitochondrial oxidative stress response (Valko et al., 2006) and presided in each B-As pro-cancer GSN (described below), *SOD2* potentially prolonged B-As cell survival and indirectly promoted an invasive cancer phenotype (Behrend et al., 2003). Elevated *SOD2* and catalase expression have been implicated in increasing proliferation and colony formation ability in As-transformed BEAS-2B cells (Chang et al., 2010). To assist in eliminating As, B-As cells favored conjugating iAs through glutathione-

mediated processes while down-regulating 7 metallothionein genes (Chilakapati et al., 2010; Salnikow and Zhitkovich, 2008). It is unclear, however, whether *PDX3* and glutathione levels within B-As cells were able to assist in protection against elevated mitochondrial ROS. Collectively, B-As cells attempted to eliminate both iAs and increased ROS, but potentially enhanced survival and promoted cancer cell-like signaling and behavior.

Altered DNA repair and epigenetic-associated B-As cell gene expression highly suggests genotoxic and epigenetic initiation MOAs following chronic As exposure. Up-regulation of several nucleotide excision, double-strand DNA repair and G1 phase checkpoint genes suggest that chronic As exposure resulted in DNA damage. As exposure can initiate ROS and DNA damage, chromosomal aberrations, and DNA repair gene expression (Chilakapati et al., 2010; Hei and Filipic, 2004). Additionally, epigenetic histone alterations (i.e. *HINFP*, *HDAC4*; Ren et al., 2011; Salnikow and Zhitkovich, 2008) and hyper- or hypomethylation of differentiation and tumor suppressor genes following arsenic exposure potentially play a role in promoting lung cancer (Helman et al., 2011; Smeester et al., 2011). It is apparent that increased mitochondrial ROS generation, DNA damage and epigenetic mechanisms influenced B-As gene transcription and signaling pathways (Gentry et al., 2010; Valko et al., 2006). Future investigations in this transformed cell model should evaluate how arsenic histone modifications and DNA methylation impact transcriptional control of key signaling pathways promoting lung cancer.

Altered peroxisome proliferator-activated receptor (*PPARα/δ*) regulation of fatty acid metabolism potentially increased proliferation and tumorigenic ability in B-As cells. *PPARα* and *PPARδ* serve crucial roles as catabolic regulators in energy metabolism and protective mediators against inflammatory signaling and hepatocarcinogenesis (Pyper et al., 2010). Previously, iAs was shown to block *PPARγ* expression via C/EBPα and Akt signaling in adipocytes. Furthermore, decreased *PPARγ* expression correlated with accelerated proliferation due to altered p21 control of the cell cycle (Wang et al., 2005; Wauson et al., 2002). In this study, over-expression of Src/MAPK, NF-κB modulators, and *NCOR1* via *HTT* down-regulation potentially altered *PPARα/δ* regulation of adipogenesis and lipid homeostasis. Decreased *PPARα/δ* expression following As exposure may represent a key regulatory switch in moving differentiated cells towards a proliferative strategy in several cancer types by increasing energy consumption (Pyper et al., 2010; Wauson et al., 2002). In summary, decreased *PPARα/δ* and increased p21 expression can potentially explain accelerated B-As proliferation and lend further support for a *PPARα/δ* and p21-mediated As carcinogenic MOA (Wauson et al., 2002). Future characterization of how chronic As exposure alters *NCOR1* and *PPARα/δ* signaling would further enhance our understanding of how As contributes to cancer and other diseases associated with fatty acid metabolism disruption.

B-As 'cancer' GSN contained evidence for both pro- and anti-cancer signaling demonstrating that As exposure to lung epithelial cells results in dysregulation of cell homeostasis. By filtering genes for 'pro-cancer' function, the presence of *IL1A*, *IL15* and neuregulin 1 (*NRG1*) driving EGFR, NF-κB, p53, migration, energy metabolism and anti-apoptotic associated signaling indicates that prolonged inflammatory signaling was primarily driving B-As cell cancer gene expression and *in vitro* phenotypic behaviors. Over-expressed *IL1A* was associated with up-regulated IKKα (*CHUK*), increased *SOD2* expression and potentially activated p38 and JNK/MAPK signaling (Reuter et al., 2010). *IL15* up-regulation affected gene expression associated with MAPK/ERK regulation (*DUSP5*), cell cycle (*CKS1B*), receptor signaling (*TNFSF10*, *TGFBR2*) and *JUN*, thus enhancing proliferation and tumorigenesis signaling. Over-expressed nucleophosmin (*NPM1*) potentially promoted transformation by altering p53 stress response and decreasing *IRF1* expression. This potentially instigated an anti-apoptotic signal by down-regulating TRAIL ligand (*TNFSF10*) in association with up-regulated *CFLAR*, a caspase 8/FADD apoptosis regulator (Fehniger and Caligiuri, 2001; Romeo et al., 2002). *NRG1* and *EGFR* over-expression altered cell signaling (*CAV1*, *TOM1L1*, *PRKAR1A*, *BCR*), stress response (*HSP90AB1*), energy production (*SLC2A3*, *PGK1*, *LDHA*), NF-κB activation (*CHUK*) and tumor-associated transcriptional regulator genes (*EGR1*, *JUN*). In comparing the 'pro-cancer' GSN to the cell behavior GSNs, these *NRG1/EGFR*-associated genes were implicated in controlling B-As colony formation, proliferation and invasion phenotypes. Arsenic exposure can over-express *NRG1* and activate ErbB family receptors (Andrew et al., 2009) which is a well-established autocrine ERK activation pathway in lung and ovarian cancer proliferation (Gollamudi et al., 2004; Simeonova and Luster, 2002; Wen et al., 2010). Furthermore, *SLC2A3*, *PGK1* and *LDHA* over-expression occurs in numerous cancers and chronically As-exposed rat lung (Fry et al., 2007; Posey et al., 2008). Lastly, altered integrin-related signaling (*ITGB5*) associated with tetraspanin (*TM4SF1*) and mitogen-responsive phosphoproteins (*DAB2* and *DAB2IP*) possibly enhanced B-As cell adhesion and invasiveness (Lekishvili et al., 2008). In summary, identification and mapping of DEG signaling relationships in a 'pro-cancer' GSN revealed potential signaling mechanisms responsible for several malignant properties of B-As cells.

B-As cell cancer-related signaling was apparent in IPA-ranked GSNs which contained genetic disorder signaling evidence associated with p21, p53, and NF-κB pathways. p21 (*CDKN1A*) and cyclin dependent kinase subunit (*CKS1B*) up-regulation associated with genes involved in p53, mRNA processing and Fe–S protein assembly signaling suggests uncontrolled progression and transition through both G1/S and G2/M phase, thus promoting B-As cell tumorigenesis (Network 1; Krishnan et al., 2010; Trouba et al., 2000; Vogt and Rossman, 2001). In addition, genes associated with cell cycle control and DNA repair (Network 8) further implicated over-expressed *NPM1*, a p53, MAPK and NF-κB regulator, as a key signaling modulator potentially enhancing B-As colony formation and proliferation (Grisendi et al., 2006). Altered p53 function was further evidenced by increased *AGR2* and decreased *SULF2* expression, key mediators of tumor growth signaling (Wang et al., 2008). Increased or decreased p21 expression, along with *CKS1B*, may represent a key step in promoting accelerated proliferation in arsenic transformed epithelial cells (Gentry et al., 2010; Wang et al., 2005; Wauson et al., 2002). Uncontrolled progression through the cell cycle with damaged DNA can lead to tumorigenesis. In addition, over-expression of several pro-inflammatory cytokines (*IL1A*, *IL15*, *NRG1*), IKKα (*CHUK*) and evidence for increased ROS production suggests activation of NF-κB, a well-known contributor to oncogenesis by providing anti-apoptosis protection (Gentry et al., 2010; Hu et al., 2002). A recent study reported similar results in that chronic $AsCl_3$-exposed BEAS-2B cells exhibited enhanced NF-κB signaling which promoted SOD2 and catalase activity in protection against ROS and contributed to colony formation and proliferation (Chang et al., 2010). Recent epidemiological gene expression profiling of infants with As-exposed mothers showed similar (i.e. *CDKN1*, NF-κB) signaling patterns (Fry et al., 2007). In summary, altered p21 and NF-κB signaling potentially represent a key step in As-promoted oncogenesis.

In addition, cancer-promoting signaling via altered MAPK signaling was evident via EF1α, Ras/MAPK, Akt and p38 MAPK-associated genes. EF1α up-regulation, a proposed oncogene that increases Akt activation (Lee and Surh, 2009), was associated with down-regulation of phospholipase C and two tumor suppressors (*TNK1*, *STK4*) that negatively regulate Ras/MAPK and apoptotic signaling (Network 2; May et al., 2010). Evidence for altered *CDK7* and p38 MAPK signaling (Networks 5 and 10) were associated with cellular stress response, inflammatory response and glutathione synthesis genes. As is a well-established inducer of several MAPK activation pathways including ERK, JNK and p38 (Simeonova and Luster, 2002). Specifically, arsenite can activate Ras/MAPK and Rac signaling via sphingosine-1-phosphate receptor stimulation, thus contributing to tumorigenic signaling with long-term activation (Druwe and Vaillancourt, 2010). In addition, over-expression of several activators and inhibitors of Akt activation further implicated Akt in potentially modulating B-As cell malignant phenotype

(Network 3). Furthermore, Akt activation is implicated in altering PPAR expression and p21 differentiation signaling (Wang et al., 2005). Over-expressed *PTEN* and *PTPRJ* potentially blocked B-As cell Ras and Akt signaling (Omerovic et al., 2010; Tokar et al., 2010b); however, it appeared not to be sufficient enough to halt malignant transformation of As-exposed BEAS-2B cells. These findings raise additional questions as to how chronic As exposure alters Ras/MAPK, p38 MAPK and Akt signaling in lung epithelial cells, thus affecting proliferation and tumor formation. Further investigation of signaling through Ras, Akt and associated upstream regulators in As-exposed lung epithelium is warranted.

Lastly, *JUN/Ap1* down-regulation protected B-As cells from superoxide ions, promoted actin-mediated survival and cell motility (Networks 7 and 9) and associated with a poor prognosis marker (*CHGA*; Gulubova and Vlaykova, 2010). Over-expressed *JUN/Ap1* can result in cell proliferation, tumorigenesis or apoptosis (Shaulian and Karin, 2002). Conversely, c-Jun down-regulation enhances *SOD2* expression during ROS generation but possibly results in low proliferation and transformation (Katiyar et al., 2010). It is possible that down-regulated c-Jun along with adequate JunB expression allowed B-As cells to transform via NF-κB and other signaling mechanisms (Hu et al., 2002; Fry et al., 2007; Passegue et al., 2002). In summary, down-regulated c-Jun promoted B-As cell survival through *SOD2* mediation of mitochondrial ROS and promoted gene expression commonly observed in cancers with poor prognosis.

In conclusion, B-As cells represent a lung cancer phenotype evidenced by enhanced cell proliferation, invasion, tumor formation and metastatic potential. Furthermore, whole genome expression profiling and *in silico* signaling pathway analysis revealed evidence for ROS generation and scavenging capacity, DNA damage, chronic inflammation via pro-inflammatory cytokine and enhanced NF-κB signaling, EGFR-regulated growth signaling, decreased *PPARα/δ* signaling, dysregulation of pro- and anti-cancer gene signaling, anti-apoptosis and invasive signaling. These cell signaling alterations represent those changes due to As_2O_3 exposure in a passaged, transformed cell line; hence caution is warranted in making comparisons to non-transformed cells. Whole genome profiling coupled with malignant cell behavior at a single, subchronic exposure time point at a realistic exposure dose allowed us to phenotypically anchor those signaling changes associated with As-exposure malignant transformation. However, gene expression can vary with dose and over time; therefore, gene signaling presented in this study should not be over-extended to other dose and time points to fully explain carcinogenic mechanism. Rather, the As-associated signaling should serve as a guide for future dose and time response studies. Follow up mechanistic studies using this established cell line will validate those signaling pathway(s) participating B-As cell malignant conversion. Since it is unclear whether As induced, enhanced or promoted BEAS-2B cell malignant transformation, future whole genome analyses should focus on dose/time response relationships to identify key molecular changes during promotion and critical dose thresholds for neoplastic transformation (Kitchin and Conolly, 2010). Future studies using B-As cells collected at earlier exposure time points will serve to address when malignant progression and promotion occurred. Gene expression from this study's B-As cell toxicogenomic profile can be compared to *in vitro*, clinical and epidemiological samples to assess model's ability to assess metal carcinogenicity and mode of action. Lastly, use of current knowledge-based microarray software, such as IPA, provides several investigative approaches to identify key GSN and potential MOAs for contaminant-exposed and transformed cell lines. Future data sets such as these may be employed as *in vitro* carcinogenesis models, assist in anti-cancer therapies and integrated into metal and metalloid risk assessments.

Conflicts of interest statement

TAS is employed by NIOSH. All other authors claim no competing conflicts of interest other than stated funding sources.

Acknowledgments

Special thanks to V. Pongrakhannon and T. Meighan for their assistance with cell culture and rtPCR analyses. The authors thank S. Talbott for helpful comments on the manuscript. YR was supported by National Institute of Health grants (R01-HL076340, R01-HL076340-04S1 and R01-HL095579). MED was funded by NIH (P20RR016477). JBB and RS were funded through the Vice President of Research Office at West Virginia University. Disclaimer: research findings and conclusions are those of the authors and do not necessarily represent the views of the National Institute for Occupational Safety and Health.

Appendix A. Supplementary data

Supplementary data to this article can be found online at http://dx.doi.org/10.1016/j.taap.2012.04.003.

References

Achanzar, W.A., Brambila, E.M., Diwan, B.A., Webber, M.M., Waalkes, M.P., 2002. Inorganic arsenite-induced malignant transformation of human prostate epithelial cells. J. Natl. Cancer Inst. 94, 1888–1891.
Andrew, A.S., Mason, R.A., Memoli, V., Duell, E.J., 2009. Arsenic activates EGFR pathway signaling in the lung. Toxicol. Sci. 109, 350–357.
ATSDR, 2007. Arsenic Toxicological Profile. U.S. Department of Human and Health Services, Washington, DC. (August).
Behrend, L., Henderson, G., Zwacka, R.M., 2003. Reactive oxygen species in oncogenic transformation. Biochem. Soc. Trans. 31, 1441–1444.
Bustamante, J., Nutt, L., Orrenius, S., Gogvadze, V., 2005. Arsenic stimulates release of cytochrome *c* from isolated mitochondria via induction of mitochondrial permeability transition. Toxicol. Appl. Pharmacol. 207, 110–116.
Carter, D.E., Aposhian, H.V., Gandolfi, A.J., 2003. The metabolism of inorganic arsenic oxides, gallium arsenide, and arsine: a toxicological review. Toxicol. Appl. Pharmacol. 193, 309–334.
Chang, Q., Pan, J., Wang, X., Zhang, Z., Chen, F., Shi, X., 2010. Reduced reactive oxygen species-generating capacity contributes to the enhanced cell growth of arsenic-transformed epithelial cells. Cancer Res. 70, 5127–5135.
Chilakapati, J., Wallace, K., Ren, H., Fricke, M., Bailey, K., Ward, W., Creed, J., Kitchin, K., 2010. Genome-wide analysis of BEAS-2B cells exposed to trivalent arsenicals and dimethylthioarsenic acid. Toxicology 268, 31–39.
Dopp, E., von Receklinghausen, U., Diaz-Bone, R., Hirner, A.V., Rettenmeier, A.W., 2010. Cellular uptake, subcellular distribution and toxicity of arsenic compounds in methylating and non-methylating cells. Environ. Res. 110, 435–442.
Druwe, I.L., Vaillancourt, R.R., 2010. Influence of arsenate and arsenite on signal transduction pathways: an update. Arch. Toxicol. 84, 585–596.
Fehniger, T.A., Caligiuri, M.A., 2001. Interleukin 15: biology and relevance to human disease. Blood 97, 14–32.
Fry, R.C., Navasumrit, P., Valiathan, C., Svensson, J.P., Hogan, B.J., Luo, M., Bhattacharya, S., Kandjanapa, K., Soontararuks, S., Nookabkaew, S., Mahidol, C., Ruchirawat, M., Samson, L.D., 2007. Activation of inflammation/NF-κB signaling in infants born to arsenic-exposed mothers. PLoS Genet. 3, e207.
Ganter, B., Giroux, C.N., 2008. Emerging applications of network and pathway analysis in drug discovery and development. Curr. Opin. Drug Discov. Devel. 11, 86–94.
Gentry, P.R., McDonald, T.B., Sullivan, D.E., Shipp, A.M., Yager, J.W., Clewell III, H.J., 2010. Analysis of genomic dose–response information on arsenic to inform key events in a mode of action for carcinogenicity. Environ. Mol. Mutagen. 51, 1–14.
Gerwin, B.I., Spillare, E., Forrester, K., Lehman, T.A., Kispert, J., Welsh, J.A., Pfeifer, A.M.A., Lechner, J.F., Baker, S.J., Vogelstein, B., Harris, C.C., 1992. Mutant p53 can induce tumorigenic conversion of human bronchial epithelial cells and reduce their responsiveness to a negative growth factor, transforming growth factor beta 1. Proc. Natl. Acad. Sci. U. S. A. 89, 2759–2763.
Gollamudi, M., Nethery, D., Liu, J., Kern, J.A., 2004. Autocrine activation of ErbB2/ErbB3 receptor complex by NRG-1 in non-small lung cancer cell lines. Lung Cancer 43, 135–143.
Grisendi, S., Mecucci, C., Falini, B., Pandolfi, P.P., 2006. Nucleophosmin and cancer. Nat. Rev. Cancer 6, 493–505.
Gulubova, M., Vlaykova, T., 2010. Expression of the xenobiotic- and reactive oxygen species-detoxifying enzymes, GST-pi, Cu/Zn SOD and Mn-SOD in the endocrine cells of colorectal cancer. Int. J. Colorectal Dis. 25, 1397–1405.
Hall, S.L., Lau, K.-H.W., Chen, S.T., Felt, J.C., Gridley, D.S., Yee, J.K., Baylink, D.J., 2007. An improved mouse Sca-1 + cell-based bone marrow transplantation model for use in gene- and cell-based therapeutic studies. Acta Haematol. 117, 24–33.
Hei, T.K., Filipic, M., 2004. Role of oxidative damage in the genotoxicity of arsenic. Free Radic. Biol. Med. 37, 574–581.
Helman, E., Naxerova, K., Kohane, I.S., 2011. DNA hypermethylation in lung cancer is targeted at differentiation-associated genes. Oncogene, http://dx.doi.org/10.1038/onc.2011.307.
Hu, Y., Jin, X., Snow, E.T., 2002. Effect of arsenic on transcription factor AP-1 and NF-kappaB DNA binding activity and related gene expression. Toxicol. Lett. 133, 33–45.

Inoue, M., Sato, E.F., Nishikawa, M., Park, A.M., Kira, Y., Imada, I., Utsumi, K., 2003. Mitochondrial generation of reactive oxygen species and its role in aerobic life. Curr. Med. Chem. 10, 2495–2505.
International Agency for Research on Cancer, 2009. IARC Special Report: Policy, a Review of Human Carcinogens—Part C: Metals, Arsenic, Dusts, and Fibers, vol. 10. IARC Press, Lyon, France, pp. 453–454.
Katiyar, S., Casimiro, M.C., Dettin, L., Ju, X.M., Wagner, E.F., Tanaka, H., Pestell, R.G., 2010. C-jun inhibits mammary apoptosis in vivo. Mol. Biol. Cell 21, 4264–4272.
Kitchin, K.T., Conolly, R., 2010. Arsenic-induced carcinogenesis-oxidative stress as a possible mode of action and future research needs for more biologically based risk assessment. Chem. Res. Toxicol. 23, 327–335.
Krishnan, A., Nair, S.A., Pillai, M.R., 2010. Loss of cks1 homeostasis deregulates cell division cycle. J. Cell. Mol. Med. 14, 154–164.
Lee, M.H., Surh, Y.J., 2009. eEF1A2 as a putative oncogene. Ann. N. Y. Acad. Sci. 1171, 87–93.
Lekishvili, T., Fromm, E., Mujoomdar, M., Berditchevski, F., 2008. The tumour-associated antigen L6 is recruited to the tetraspanin-enriched microdomains: implication for tumour cell motility. J. Cell Sci. 121, 685–694.
May, W.S., Hoare, K., Hoare, S., Reinhard, M.K., Lee, Y.J., Oh, S.P., 2010. Tnk1/Kos1: a novel tumor suppressor. Trans. Am. Clin. Climatol. Assoc. 121, 281–292.
National Research Council, 2001. Arsenic in Drinking Water. National Academy of Sciences, Washington, DC.
Offergelt, J.A., Roels, H., Buchet, J.P., Boeckx, M., Lauwerys, R., 1992. Relation between airborne arsenic trioxide and urinary excretion of inorganic arsenic and its methylated metabolites. Br. J. Ind. Med. 49, 387–393.
Omerovic, J., Claque, M.J., Prior, I.A., 2010. Phosphatome profiling reveals PTPN2, PTPRJ, and PTEN as potent negative regulators of PKB/Akt activation in Ras-mutated cancer cells. Biochem. J. 426, 65–72.
Passegue, E., Jochum, W., Behrens, A., Ricci, R., Wagner, E.F., 2002. JunB can substitute for Jun in mouse development and cell proliferation. Nat. Genet. 30, 158–166.
Payne, S., 2005. Gender in Lung Cancer and Smoking Research. World Health Organization, p. 43.
Pershagen, G., Nordberg, G., Bjorklund, N.E., 1984. Carcinomas of the respiratory tract in hamsters given arsenic-trioxide and/or benzo[a]pyrene by the pulmonary route. Environ. Res. 34, 227–241.
Pi, J., Diwan, B.A., Sun, Y., Liu, J., Qu, W., He, Y., Styblo, M., Waalkes, M.P., 2008. Arsenic-induced malignant transformation of human keratinocytes: involvement of Nrf2. Free Radic. Biol. Med. 45, 651–658.
Posey, T., Weng, T., Chen, Z., Chintagari, N.R., Wang, P., Jin, N., Stricker, H., Liu, L., 2008. Arsenic-induced changes in gene expression of lung epithelial L2 cells: implications in carcinogenesis. BMC Genomics 9, 115.
Putila, J.J., Guo, N.L., 2011. Association of arsenic exposure with lung cancer incidence rates in the United States. PLoS One 6, e25886.
Pyper, S.R., Viswakarma, N., Yu, S., Reddy, J.K., 2010. PPARalpha: energy combustion, hypolipidemia, inflammation and cancer. Nucl. Recept. Signal. 8, e002.
Ren, X., McHale, C.M., Skibola, C.F., Smith, A.H., Smith, M.T., Zhang, L., 2011. An emerging role for epigenetic dysregulation in arsenic toxicity and carcinogenesis. Environ. Health Perspect. 119, 11–19.
Reuter, S., Gupta, S.C., Chaturvedi, M.M., Aggarwal, B.B., 2010. Oxidative stress, inflammation, and cancer: how are they linked? Free Radic. Biol. Med. 49, 1603–1616.
Romeo, G., Fiorucci, G., Chiantore, M.V., Percario, Z.A., Vannucchi, S., Affabris, E., 2002. IRF-1 as a negative regulator of cell proliferation. J. Interferon Cytokine Res. 22, 39–47.
Salnikow, K., Zhitkovich, A., 2008. Genetic and epigenetic mechanisms in metal carcinogenesis and cocarcinogenesis: nickel, arsenic and chromium. Chem. Res. Toxicol. 21, 28–44.
Shaulian, E., Karin, M., 2002. AP-1 as a regulator of cell life and death. Nat. Cell Biol. 4, E131–E136.
Simeonova, P.P., Luster, M.I., 2002. Arsenic carcinogenicity: relevance of c-Src activation. Mol. Cell. Biochem. 234, 277–282.
Smeester, L., Rager, J.E., Bailey, K.A., Guan, X., Smith, N., Garcia-Vargas, G., Del Razo, L.-M., Drobna, Z., Kelkar, H., Styblo, M., Fry, R., 2011. Epigenetic changes in individuals with arsenicosis. Chem. Res. Toxicol. 24, 165–167.
Smith, T.J., Crecelius, E.A., Reading, J.C., 1977. Airborne arsenic exposure and excretion of methylated arsenic compounds. Environ. Health Perspect. 19, 89–93.
States, J.C., Barchowsky, A., Cartwright, I.L., Reichard, J.F., Futscher, B.W., Lantz, R.C., 2011. Arsenic toxicology: translating between experimental models and human pathology. Environ. Health Perspect. 119, 1356–1363.
Straif, K., Benbrahim-Talla, L., Baan, R., Grosse, Y., Secretan, B., El Ghissassi, F., Bouvard, V., Guha, N., Freeman, C., Galichet, L., Cogliano, V., WHO International Agency for Research on Cancer Monograph Working Group, 2009. A review of human carcinogens-Part C: metals, arsenic, dusts and fibres. Lancet Oncol. 10, 453–455.
Sun, H., Clancy, H.A., Kluz, T., Zavadil, J., Costa, M., 2011. Comparison of gene expression profiles in chromate transformed BEAS-2B cells. PLoS One 6, e17982.
Thomas, D.J., Styblo, M., Lin, S., 2001. The cellular metabolism and systemic toxicity of arsenic. Toxicol. Appl. Pharmacol. 176, 127–144.
Tokar, E.J., Benbrahin-Tallaa, L., Ward, J.M., Lunn, R., Sams, R.L., Waalkes, M.P., 2010a. Cancer in experimental animals exposed to arsenic and arsenic compounds. Crit. Rev. Toxicol. 40, 912–927.
Tokar, E.J., Diwan, B.A., Waalkes, M.P., 2010b. Arsenic exposure transforms human epithelial stem/progenitor cells into a cancer-like phenotype. Environ. Health Perspect. 118, 108–115.
Trouba, K.J., Wauson, E.M., Vorce, R.L., 2000. Sodium arsenite-induced dysregulation of proteins involved in proliferative signaling. Toxicol. Appl. Pharmacol. 164, 161–170.
Ullmann, R., Bongiovanni, M., Halbwedl, I., Petzmann, S., Gogg-Kammerer, M., Sapino, A., Papotti, M., Bussolati, G., Popper, H.H., 2003. Bronchiolar columnar cell dysplasia-genetic analysis of a novel preneoplastic lesion of peripheral lung. Virchows Arch. 442, 429–436.
Valko, M., Rhodes, C.J., Moncol, J., Izakovic, M., Mazur, M., 2006. Free radicals, metals and antioxidants in oxidative stress-induced cancer. Chem. Biol. Interact. 160, 1–40.
Vogt, B.L., Rossman, T.G., 2001. Effects of arsenic on p53, p21 and cyclin D expression in normal human fibroblasts—a possible mechanism for arsenite's comutagenicity. Mutat. Res. 478, 159–168.
Wang, Z.H., Jiang, C.S., Liu, L., Wang, X.H., Jin, H.J., Wu, Q., Chen, Q., 2005. The role of Akt on arsenic trioxide suppression of 3T3-L1 preadipocyte differentiation. Cell Res. 15, 379–386.
Wang, Z., Hao, Y., Lowe, A.W., 2008. The adenocarcinoma-associated antigen, AGR2, promotes tumor growth, cell migration, and cellular transformation. Cancer Res. 68, 492–497.
Wang, L., Luanpitpong, S., Castranova, V., Tse, W., Lu, Y., Pongrakhananon, V., Rojanasakul, Y., 2011. Carbon nanotubes induce malignant transformation and tumorigenesis of human lung epithelial cells. Nano Lett. 11, 2796–2803.
Wauson, E.M., Langan, A.S., Vorce, R.L., 2002. Sodium arsenite inhibits and reverses expression of adipogenic and fat cell-specific genes during *in vitro* adipogenesis. Toxicol. Sci. 65, 211–219.
Wen, G., Calaf, G.M., Partridge, M.A., Echiburu-Chau, C., Zhao, Y., Huang, S., Chai, Y., Li, B., Hu, B., Hei, T.K., 2008. Neoplastic transformation of human small airway epithelial cells induced by arsenic. Mol. Med. 14, 2–10.
Wen, G., Hong, M., Calaf, G.M., Roy, D., Partridge, M.A., Hei, T.K., 2010. Phosphoproteomic profiling of arsenite-treated human small airway epithelial cells. Oncol. Rep. 23, 405–412.
World Health Organization, 2001. Environmental Health Criteria 224: Arsenic and Arsenic Compounds. Washington, DC.